Physico-chemical characterization of ferrocenyl-modified hyperbranched poly(ethylenimine) self-assembled multilayers

CrossMark

María V. Bracamonte [a], Claudia Yañez [b], Soledad Bollo [b], Gustavo A. Rivas [a], Nancy F. Ferreyra [a,*]

[a] INFIQC, Departamento de Fisicoquímica, Facultad de Ciencias Químicas, Universidad Nacional de Córdoba, 5000 Córdoba, Argentina
[b] Laboratorio de Bioelectroquímica, Facultad de Ciencias Químicas y Farmacéuticas, Universidad de Chile, Santiago, Chile

ARTICLE INFO

ABSTRACT

In this work, we characterize the electrochemical behavior of a new ferrocenyl-modified, hyperbranched poly(ethylenimine) (HBPei-Fc). The effects of the ionic strength, pH and the nature of the anion of the supporting electrolyte on the electrochemical behavior of the redox polymer were studied using cyclic voltammetry and an electrochemical quartz crystal microbalance. The interactions of the polymer with the anions of the supporting electrolyte, which was incorporated during the redox process, determined the electrochemical behavior that was observed. The polymer was employed for the construction of layer-by-layer-assembled multi-composite films using thiolated gold surfaces with HBPei-Fc as the poly-cation and citrate-stabilized gold nanoparticles or glucose oxidase (GOx) as the negative polyelectrolyte. The self-assembled multilayers were characterized using UV–Vis spectrophotometry and electrochemical techniques to follow the signal of the ferrocene groups of the polymer. The adsorption of the polymer and GOx was analyzed using surface plasmon resonance to determine the surface coverage and the kinetic properties of the process. The results demonstrated that the ferrocenyl-modified polymer is an efficient platform for the immobilization of both inorganic materials, such as metallic nanoparticles, and biomolecules.

1. Introduction

Redox polymers are characterized by functional groups in their backbones that can be reversibly reduced or oxidized. Charge transport in these polymers occurs through electron hopping between neighboring redox sites, physical diffusion of redox sites or a combination of these two mechanisms [1]. The movement of counter ions is associated with charge transfer during the electrochemical reaction to maintain electroneutrality. Consequently, the conditions of the medium, such as the nature of the supporting electrolyte, pH and ionic strength, as well as the polymer properties (e.g., conformation, chain and segmental motions and morphology), play a fundamental role in their electrochemical response [1].

Redox polymers have been extensively employed in the construction of layer-by-layer (LbL) self-assembled structures. Several examples of structures containing redox groups, such as viologen [2], Prussian blue [3], poly(thiophene) [4] and osmium bipyridyl complex (Os-bpy) [5], have been reported for potential applications in mechanical actuators, sensors, photochromic devices and, more recently, for surface-mediated controlled drug release [6].

Specifically, ferrocene-modified polymers have been extensively studied because of their interesting reactivity and redox behavior, among other properties [7]. Two strategies have been attempted to obtain ferrocene-derivatized polymers: substitution of functional groups in polymers without redox behavior, such as poly(4-vinylpyridine) [8], chitosan [9], poly N-isopropylacrylamide [10] and poly(allylamine) [11], and the synthesis of redox copolymers in which ferrocene was covalently attached, such as poly(vinylferrocene-co-2-hydroxyethyl methacrylate) [12], poly(N-acryloylpyrrolidine-co-vinylferrocene), acrylamide copolymers [13], ferrocene-based peptide/amides [14] and poly(glycidyl methacrylate-co-vinylferrocene) [15].

Due to ferrocene's standard redox potential, ferrocene-modified polymers are appropriate as mediators for glucose oxidase in amperometric glucose biosensors [16,17].

Schmidtke and co-workers have studied a series of redox polymers based on linear poly(ethylenimine) and ferrocene (Fc-C6-LPEI) for use in glucose biosensors [18,19] and biofuel cell anodes [20]. Recently, they studied layer-by-layer assembled structures of Fc-C6-LPEI with poly(acrylic acid), poly(glutamic acid) or glucose oxidase, demonstrating that the formation of the film was dependent upon the nature of the anionic polyelectrolyte [21].

---

* Corresponding author. Tel.: +54 351 4334169; fax: +54 351 4334188.
E-mail addresses: vbracamonte@fcq.unc.edu.ar (M.V. Bracamonte), cyanez@ciq.uchile.cl (C. Yañez), sbollo@ciq.uchile.cl (S. Bollo), grivas@fcq.unc.edu.ar (G.A. Rivas), ferreyra@fcq.unc.edu.ar (N.F. Ferreyra).

Xu and co-workers have reported the fabrication and characterization of multilayer films based on layer-by-layer assembly of ferrocene poly(ethylenimine) and gold nanoparticles. The multilayers were applied to analyze its electrocatalytic response towards the oxidation of ascorbic acid and the reduction of oxygen [22].

All the cited examples show that the synthesis and application of ferrocenyl-functionalized polymers are of interest to many fields, such as electrochemistry, materials science, organic synthesis and catalysis. The development of novel redox polymers continues to be an important area of research in the field of bioelectronics [23].

In this work, we present the synthesis and characterization of a new ferrocenyl-modified polymer obtained from hyperbranched poly(ethylenimine) (HBPei), named HBPei-Fc. The goal of this work was to study the electrochemical behavior of the polymer and evaluate the effect of the anion of the supporting electrolyte, pH and ionic strength on the electrochemical response. Based on the interesting molecular structure and resulting high charge density, the second goal of our work was to evaluate the construction of multi-composite films built using electrostatic layer-by-layer assembly of HBPei-Fc as the polycation and citrate-stabilized gold nanoparticles or glucose oxidase as the negative polyelectrolytes. The resulting structures were characterized using UV–Vis spectrophotometry, scanning electron microscopy, surface plasmon resonance, electrochemical-quartz crystal microbalance and cyclic voltammetry.

2. Materials and methods

2.1. Reagents

Citrate-stabilized gold nanoparticles (Au-NPs) with a 15-nm average diameter were synthesized using the Turkevich method. The diameter of the Au-NPs was determined using the Khlebtsov method [24] (considering the experimentally determined value of the maximal absorbance, λ_{max} = 520 nm). The glucose oxidase (GOx) (Type X-S, Aspergillus niger, EC 1.1.3.4, 210,000 units per gram of solid, Mw = 160 kDa) and hyperbranched polyethylenimine (HBPei, average Mw = 750 kDa) were from Sigma. The sodium 3-mercapto-1-propanesulfonate (MPS), ferrocenecarboxaldehyde and sodium borohydride were from Aldrich. Other chemicals were reagent grade and were used without further purification. All solutions were prepared with ultra-pure water (18 MΩ cm) from a MilliRO–MilliQ system.

2.2. Synthesis and characterization of ferrocenyl-modified hyperbranched polyethylenimine

The synthesis of HBPei-Fc was performed as described in [25]. The presence of ferrocenyl groups in the synthesized polymer was corroborated using UV–Vis experiments (see Fig. S1 of Supporting information). The substitution degree (SD) of amine hydrogen by ferrocenylmethylene moieties was determined using ^{1}H Nuclear Magnetic Resonance spectra from the integration ratio of the ferrocenyl proton to the polymer methylene backbone signals (Fig. S2 of Supporting information). The value was 28.4%, which is in good agreement with the value reported for linear polyethylenimine (av. MW = 86.000) and branched polyethylenimine of low molecular weight (av. MW = 200.000) [25].

2.3. Equipment

UV–Vis experiments were performed with a Shimadzu UV1601 Spectrophotometer using a quartz cuvette with a 1.0 or 0.1 cm path length. Cyclic voltammetry (CV) was performed with an Autolab PGSTAT 128N potentiostat (Metrohm Autolab B.V.). Gold disk electrodes (Au) of 2 mm diameter (Model CHI 101) were used as the substrates. A platinum wire and an Ag/AgCl, 3 mol dm^{-3} NaCl electrode (Model RE-5B, BAS) were used as the counter and reference electrodes, respectively. All reported potentials are referred to this reference electrode. Electrochemical-quartz crystal microbalance (EQCM) measurements were conducted with a CHI 400 Time-Resolved EQCM System (CHI). Quartz disks coated with gold (Model CHI 125A, 0.196 cm^2 of area) were used as substrates. The experiments were performed at room temperature. Surface plasmon resonance (SPR) measurements were conducted with a single channel Autolab SPRINGLE instrument (Metrohm Autolab B.V). SPR sensor disks (Model BK 7) were mounted on a hemi-cylindrical lens through index-matching oil to form the base of a cuvette. Sample solutions (100 μL) were injected automatically into the cuvette. The measurements were conducted under non-flow liquid conditions with the cuvette thermostated at 25 °C.

2.4. Surface modification

Clean gold surfaces were immersed in a fresh 2.00×10^{-2} M MPS solution prepared in 1.60×10^{-3} M sulfuric acid solution, followed by careful rinsing with deionized water. Adsorption of HBPei-Fc was performed over 15 min from a 3.0 mg mL^{-1} polymer solution prepared in a 0.200 M acetate buffer solution pH 5.00. After the adsorption step, surfaces were copiously rinsed with acetate buffer solution. The resulting electrodes are indicated as Au/MPS/HBPei-Fc.

Adsorption of Au-NPs was performed by immersion of the Au/MPS/HBPei-Fc surfaces in the colloidal Au-NPs solution for the specified time. After each adsorption step, surfaces were copiously rinsed with deionized water. Multilayered films were constructed by alternate immersion of Au/MPS substrates in HBPei-Fc and Au-NPs solutions for the selected time. These structures are named Au/MPS/(HBPei-Fc/Au-NPs)$_n$, with n being the number of HBPei-Fc/Au-NPs adsorption steps.

For UV–Vis measurements, the internal surface of the quartz cuvette (Quartz) was treated by sonication for 20 min in an ethanolic solution of NaOH 1.0% w/v to expose negative charges. Adsorption of HBPei-Fc and Au-NPs was performed by filling the cuvette with each solution for a predetermined time. Then, the solutions were removed, and the cuvette was repeatedly washed with deionized water. UV–Vis measurements were performed in deionized water to avoid modification by surface drying. These structures are named Quartz/(HBPei-Fc/Au-NPs)$_n$, where n is the number of HBPei-Fc/Au-NPs adsorption steps.

Adsorption of GOx was performed by immersion of Au/MPS/HBPei-Fc surfaces in 1.0 mg mL^{-1} GOx solution prepared in 0.050 M phosphate buffer solution at pH 7.40 for 30 min, followed by copiously rinsing with phosphate buffer solution. The structures are denoted as Au/MPS/(HBPei-Fc/GOx)$_m$, where m is the number of HBPei-Fc/GOx adsorption steps.

3. Results and discussion

3.1. Electrochemical response of HBPei-Fc

3.1.1. Adsorption of HBPei-Fc

We evaluate the adsorption process using SPR to determine the concentration and adsorption time of HBPei-Fc for further construction of self-assembled multilayers. Fig. 1 presents the sensorgram obtained during the adsorption of the polymer at the Au/MPS surface. The experiment starts recording a baseline in a 0.200 M acetate buffer solution at pH 5.00. Next, a 3.0 mg mL^{-1} HBPei-Fc solution is injected into the cuvette, and a fast increase in the
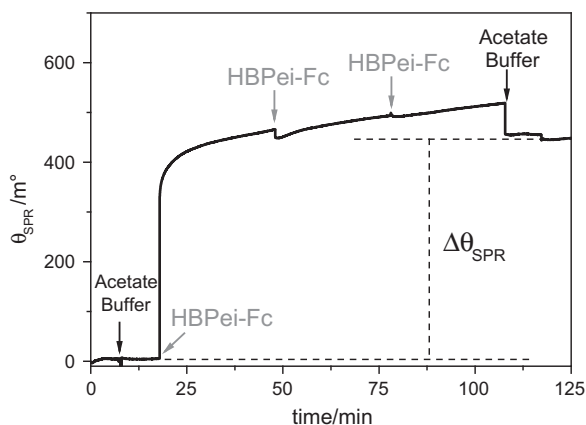
Fig. 1. Sensorgram obtained during the adsorption of HBPei-Fc at Au/MPS. Arrows indicate the addition to the cuvette of 3.0 mg mL^{-1} HBPei-Fc solution (gray) and 0.200 M acetate buffer solution at pH 5.00 (black).

resonance angle is observed because of the polymer adsorption. From the sensorgram, it is clear that the stationary value of SPR signal is reached after 15 min and that 90% of the mass of the polymer is adsorbed during the first 5 min. Two more additions of HBPei-Fc solution do not produce significant changes in the SPR signal, indicating that the maximum surface coverage was reached with only one addition of the polymer to the cuvette. To remove the weakly bound polymer, the surface was washed with 0.200 M acetate buffer solution at pH 5.00 until a stationary response was obtained. The variation of the SPR angle, $\Delta\theta_{SPR}$, (the difference in the signal recorded in buffer before and after the polymer adsorption [26]) was $(4 \pm 1) \times 10^2$ m°, which corresponds to a polymer surface coverage of $\Gamma_{HBPei-Fc}$ of $(3.7 \pm 0.8) \times 10^2$ ng cm^{-2}. From these results, an adsorption time of 15 min and a solution concentration of 3.0 mg mL^{-1} were selected for further experiments.

3.1.2. Electrochemical response of HBPei-Fc

The electrochemical response of the adsorbed polymer was studied using CV. Fig. 2A shows the response at Au/MPS (dashed line) and Au/MPS/HBPei-Fc (solid line) electrodes in 0.200 M NaClO$_4$ solution pH 6.00 at a scan rate, v, of 0.100 V s^{-1}. At Au/MPS, only capacitive currents, i_{cap}, are observed in the studied potential range. A capacitance value $C_{dl} = (20 \pm 5)$ μF cm^{-2} was obtained from the plot of i_{cap} vs. v measured at 0.060 V (vs. Ag/AgCl/3 mol dm^{-3} NaCl electrode), in good agreement with previous reports [27]. An equivalent analysis was performed for the i_{cap} measured at 0.060 V on Au/MPS/HBPei-Fc; under this potential no faradaic contribution to the current is observed. The measured value was $C_{dl} = (12 \pm 2)$ μF cm^{-2}. The decrease of C_{dl} in the presence of HBPei-Fc indicates the formation of a compact structure on the electrode surface that decreases the dielectric constant at the electrode/solution interface. In addition, a faradaic process is observed after the adsorption of HBPei-Fc that corresponds to the oxidation and reduction of ferrocenyl groups of the polymer. For this process, the $E_{app}^{1/2}$, calculated as $E_{app}^{1/2} = 1/2 E^{ox} + 1/2 E^{red}$, is (0.38 ± 0.03) V, and the full width at half oxidation peak height (FWHH) is (0.18 ± 0.01) V. The increase in FWHH, compared to the theoretical value 0.0906 V expected for a surface-confined redox process involving one electron, could be attributed to repulsive interactions between neighboring ferrocenyl groups [28] or modifications in the local environment [29]. The variation of the anodic peak current, i_{pa}, with v is displayed in the inset of Fig. 2A. The surface concentration of the electroactive polymer $\Gamma_{HBPei-Fc^*} = (6.0 \pm 0.6) \times 10^{-11}$ mol cm^{-2} was determined from the slope and considering the following reaction and Eq. (1) [30]:
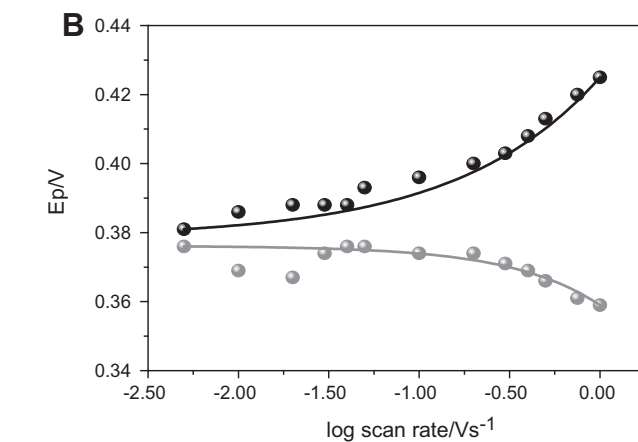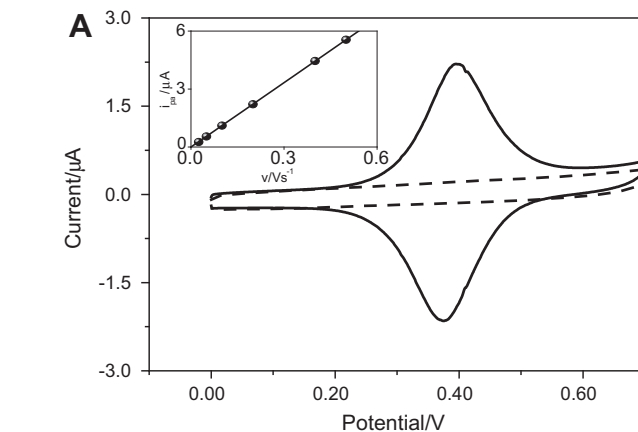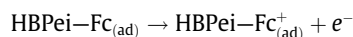

Fig. 2. (A) Cyclic voltammograms obtained at Au/MPS (dashed line) and Au/MPS/HBPei-Fc (solid line) at $v = 0.100$ V s^{-1}. The inset shows the variation of i_{pa} of Au/MPS/HBPei-Fc vs. v. (B) Anodic (●) and cathodic (●) peak potentials of Au/MPS/HBPei-Fc as a function of log v. The supporting electrolyte is 0.200 M NaClO$_4$ at pH 6.00. The potential (V) is reported vs. (Ag/AgCl/3 mol dm^{-3} NaCl).

$$HBPei-Fc_{(ad)} \rightarrow HBPei-Fc^+_{(ad)} + e^-$$

$$i_p = \frac{n^2 F^2}{4RT} v A \Gamma^*_{BPei-Fc} \tag{1}$$

where A is the electroactive area and other symbols have their usual meaning.

The heterogeneous rate constant, k, and the transference coefficient, α, of the redox process of ferrocenyl groups immobilized on the electrode surface was calculated from the cyclic voltammograms using Laviron theory [31]. For this purpose, we analyzed the variation of the peak potential, E_p, with the logarithm of v. Fig. 2B shows plots of the anodic and cathodic peak potentials as a function of the logarithm of v for the Au/MPS/HBPei-Fc electrode. It is clear that E_{pc}, E_{pa} and peak potential separation (ΔE_p) are practically invariant with v when the latter is low enough, i.e., $v < 0.040$ V s^{-1}. In contrast, at sweep rates higher than 0.200 V s^{-1}, E_{pc} and E_{pa} shift negatively and positively, respectively, and ΔE_p increases proportionally to the logarithm of v. This result demonstrates a thin layer characteristics at a small scan rate and a quasi-reversible behavior at a high scan rate. The slopes of the straight lines are $m_a = 2.3\ RT/(1-\alpha)nF$ and $m_c = 2.3\ RT/\alpha nF$ for the anodic and cathodic processes, respectively. The rate constant can be determined from their intersection point [31]. The calculated transfer coefficient and heterogeneous electron transfer rate constant were (0.59 ± 0.01) and (1.50 ± 0.05) s^{-1}, respectively.

3.1.3. Effect of the supporting electrolyte on the electrochemical response of HBPei-Fc

The HBPei-Fc oxidation process generates positive charges in the polymer layer, which have to be compensated by incorporating counter ions from the solution to preserve the charge neutrality. Therefore, the mobility of the counter ions through the film could limit the rate of the charge transfer process [28]. This effect was analyzed by EQCM studies. The method is suitable for a quantitative analysis of the changes associated with faradaic processes produced in a rigid mass at a quartz crystal electrode using Sauerbrey's equation [32]. The mass changes monitored by EQCM can be related to the electric charge, Q, involved in the electrode reactions using Faraday's laws.

Fig. 3 compares the cyclic voltammograms (A) and the changes in the frequency (B) of the electrochemical response of the Au/MPS/HBPei-Fc electrodes measured in 0.200 M NaClO$_4$ at pH = 6.00 (solid line) and 0.200 M phosphate buffer solutions at pH = 6.00 (dashed line). In NaClO$_4$ solution, a ratio of $i_{pa}/i_{pc} = 1.4$, a $\Delta E_p = 0.030$ V and a FWHH of 0.150 V are observed. A decrease in i_{pc}, a negative shift in E_{pc} and an increase in ΔE_p up to 0.080 V are observed in phosphate buffer solution. Fig. 3B shows that the frequency decreases, independently of the medium, during the oxidation process. This effect is caused by the increase in the mass in the polymeric layer due to the incorporation of hydrated anions from the solvent to compensate the positive charges generated in the ferrocenium groups. During the cathodic scan, these groups are reduced, and the anions and water are expelled into the solution, which results in an increase of frequency [2,33–35]. The changes in frequency between the stationary values, Δf, were −15.6 Hz and −40.7 Hz for NaClO$_4$ and phosphate buffer solutions, respectively. Additionally, a hysteresis in the frequency between the forward and backward scan is observed in the phosphate buffer, indicating that solvated phosphate anions are partially retained by the polymer. The interactions of the anions of the supporting electrolyte with the polymer are responsible for this effect. It is important to remark that phosphate anions, in addition to the electrostatic interactions, can establish H-bridges with the amine groups of the polymer [19,36]. Because of these strong interactions, the reduction process of HBPei-Fc$^+$ is less favorable in this medium and requires more energy.

Applying Sauerbrey's equation, the mass exchange produced during the oxidation process was estimated. From the slope of the mass vs. charge plots (Figs. S3 and S4 of the Supporting

information), values of 130.3 g and 255.7 g per mol of charge were calculated for NaClO$_4$ and phosphate, respectively. Taking into account the molar mass of each anion, we determined that 2 and 9 mol of water are incorporated into the structure per mol of oxidized HBPei-Fc for the NaClO$_4$ and phosphate buffer solutions, respectively. Therefore, the differences in Δf observed during the oxidation process are clearly due to the solvation of each anion.

The influences of the supporting electrolyte concentration and pH were also evaluated. Table 1 summarizes the values of $E_{app}^{1/2}$ and normalized i_{pa} obtained at different ionic strengths. Cyclic voltammograms were recorded in NaClO$_4$ solution at pH = 6.00 and $v = 0.100$ V s^{-1}. As the ionic strength increases, the normalized i_{pa} (with respect to the response at 0.05 M NaCl) decreases, and the $E_{app}^{1/2}$ shifts toward lower energy values. This tendency can be attributed to the Donnan potential difference, $\Delta\phi_D$, originating at the polymer/solution interface, which depends on the electrolyte concentration in solution and the concentration of fixed charges in the polymer [37]. The $E_{app}^{1/2}$ reported vs. the reference electrode is given by $E_{app}^{1/2} = E^{0\prime} + \Delta\phi_D$, where $E^{0\prime}$ is the formal redox potential of the ferrocenium/ferrocene redox couple in the absence of electric work. In this experiment, the positive charges of the polymer are fixed (pH is constant). Accordingly, the decrease in $E_{app}^{1/2}$ is related to the decrease in $\Delta\phi_D$ as the ionic strength increases, as expected for a process that involves the exchange of anions. In addition, as the concentration of ions in solution increases, the thickness of the films increases due to the hydration of the polymer, and a decrease of i_{pa} is observed [38].

The effect of the supporting electrolyte solution pH on the voltammetric response of Au/MPS/HBPei-Fc was also evaluated. Solutions of NaClO$_4$ at a concentration of 0.200 M, constant ionic strength and a pH between 3.50 and 9.50 were used as electrolytes. No variations in the response were observed under the explored conditions (not shown). Similar experiments were performed in 0.200 M phosphate buffer solution with a pH between 5.00 and 11.20. Table 2 summarizes the parameters obtained. A shift of $E_{app}^{1/2}$ to less positive values is evident. Anodic peak currents are almost constant, but a clear decrease of i_{pc} is observed as the pH of the solution increases. This effect cannot be attributed to the deprotonation of the polymer because it was not observed in the experiments performed in NaClO$_4$ solution over the same range of pH. At pH > 8.50, anionic HPO$_4^{2-}$ predominates in solution and forms ionic par with ferrocenium groups of the polymer [19,36]. This strong interaction makes the expulsion of the ions from the film difficult, which is necessary during the reduction process. This effect was also shown using EQCM experiments (not shown).
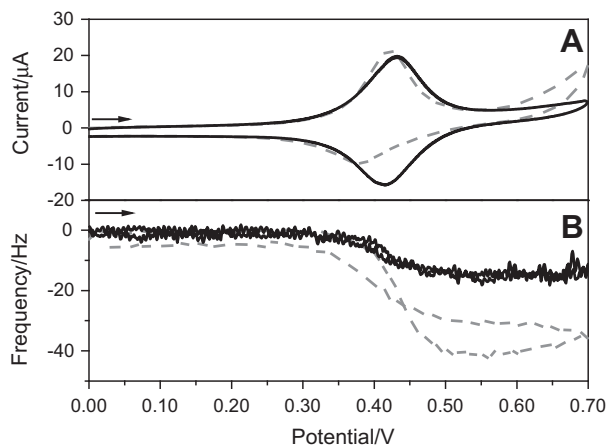
3.2. Evaluation of HBPei-Fc as a platform for the adsorption of gold nanoparticles

The adsorption of gold nanoparticles onto HBPei-Fc was evaluated using UV–Vis absorption spectroscopy, SEM and cyclic voltammetry.

Fig. 3. Current (A) and frequency (B) response of Au/MPS/HBPei-Fc electrodes as a function of the applied potential at $v = 0.100$ V s^{-1}. The arrows indicate the sweep potential direction. Supporting electrolyte: 0.200 M NaClO$_4$ at pH 6.00 (solid line) and 0.200 M phosphate buffer at pH 6.00 (dashed line). The potential (V) is reported vs. (Ag/AgCl/3 mol dm^{-3} NaCl).

Table 1
Ionic strength effect on HBPei-Fc electrochemical response.

[NaClO$_4$]/M	$E_{app}^{1/2}$/V[a]	i_{pa}[b]
0.05	0.43 ± 0.03	1.00
0.10	0.41 ± 0.03	0.90
0.20	0.40 ± 0.03	0.82
0.40	0.39 ± 0.03	0.73

[a] Values determined from cyclic voltammograms were performed in NaClO$_4$ solution pH 6.00 at 0.100 V s^{-1}, and reported vs. Ag/AgCl/3 mol dm^{-3} NaCl.
[b] Normalized by i_{pa} value of the experiment performed at 0.050 M NaClO$_4$ solution.

pH	Ionic strength	$E_{app}^{1/2}$/V	i_{pa}/μA	i_{pc}/μA
5.00	0.20	0.42 ± 0.02	4.8 ± 0.1	2.4 ± 0.6
6.00	0.22	0.39 ± 0.03	4.6 ± 0.1	1.8 ± 0.2
8.90	0.49	0.33 ± 0.02	4.6 ± 0.1	0.9 ± 0.1
11.20	0.54	0.31 ± 0.03	4.5 ± 0.1	0.8 ± 0.1

[a] Values determined from cyclic voltammograms were performed in 0.200 M phosphate buffer solution at 0.100 V s^{-1} and reported vs. Ag/AgCl/3 mol dm^{-3} NaCl.

3.2.1. UV–Vis characterization

Fig. 4A shows the UV–Vis absorption spectra of Quartz/HBPei-Fc (dashed lines) and Quartz/(HBPei-Fc/Au-NPs) (solid lines) as a function of the interaction time (t) of Au-NPs with HBPei-Fc at modified quartz. One broad band due to the SPR of Au-NPs is observed in the region of 500–700 nm. A red shift of λ_{max} is observed compared to colloidal Au-NPs solution (λ_{max} = 520 nm); the SPR band of Au-NPs ranged from 528 nm to 544 nm for 15 and 120 min, respectively. This effect can be attributed to changes in the dielectric environment as the Au-NPs surface coverage increases [39]. Fig. 4B shows the evolution of the maximum SPR absorbance (Abs_{max}) as a function of t. A linear increase of Abs_{max} is observed up to 60 min, and a plateau value is reached after 120 min. The surface distribution of the Au-NPs adsorbed on Au/MPS/HBPei-Fc was analyzed using SEM. Fig. S5 of the Supporting information demonstrates the attachment of Au-NPs onto HBPei-Fc-modified gold substrates after 30 (A) and 90 (B) min of Au-NPs adsorption. In both experiments, a homogeneous distribution is observed, and most Au-NPs are adsorbed as isolated particles.

Self-assembled multilayers were built by exposing HBPei-Fc and Au-NPs to 15 min and 30 min of adsorption, respectively. Fig. 4C shows UV–Vis spectra obtained as the number of bilayers, n, of HBPei-Fc/Au-NPs increases from 1 to 8. Fig. 4D shows the variation in Abs_{max} vs. n. The intensity of the SPR band rises linearly as the number of dipping cycles increases, indicating that a constant number of Au-NPs is immobilized in each layer [40]. Because the maximum coverage of Au-NPs is mainly dependent on the coverage of HBPei-Fc, this result indicates good reproducibility in the alternate adsorption of polymer and Au-NPs. In contrast to the monolayer spectrum, multilayered structures show a strongly redshifted SPR signal (up to ∼600 nm) as n increases, suggesting Au-NPs aggregation or interactions between Au-NPs of different layers. Similar results have been reported for Au-NPs in self-assembled multilayers [41].

3.2.2. Electrochemical characterization

Fig. 5A shows cyclic voltammograms obtained at Au/MPS/(HBPei-Fc/Au-NPs)$_n$/HBPei-Fc electrodes with an increasing number of bilayers recorded at 0.100 V s^{-1} in a 0.200 M NaClO$_4$ solution at pH 6.00. Fig. 5B shows i_{pa} as a function of n. A linear relationship is observed up to n = 6, which slightly decreases for larger n. This result is a clear indication that similar amounts of HBPei-Fc were incorporated in each adsorption cycle and also that the electrochemical connection between the electrode and the polymer redox moieties was maintained throughout the film. The electron transfer between Fc on multilayered films and the electrode may be attributed mainly to a hopping mechanism favored by the connection of neighboring redox groups of HBPei-Fc due to the interpenetration between layers in the film and the presence of Au-NPs.

The incorporation of gold nanoparticles in self-assembled structures improves charge transference through films [42,43]. It could also facilitate the connection between redox centers of the polymer. To confirm this hypothesis, using SECM, we evaluate the differences in the electrochemical response of ferrocenemethanol (FcMOH) at Au, Au/MPS/HBPei-Fc and Au/MPS/(HBPei-Fc/Au-NPs)$_1$. The results show an increase in surface reactivity after the adsorption of gold nanoparticles (Fig. S6) and are in agreement with the conclusions from Fig. 5.

3.3. Evaluation of HBPei-Fc as a platform for the adsorption of glucose oxidase

Given the results of the successful formation of multilayers of HBPei-Fc/Au-NPs by electrostatic assembly as described above, we evaluate the possibility of using HBPei-Fc as a platform for the adsorption of biomolecules. We use the enzyme GOx as a
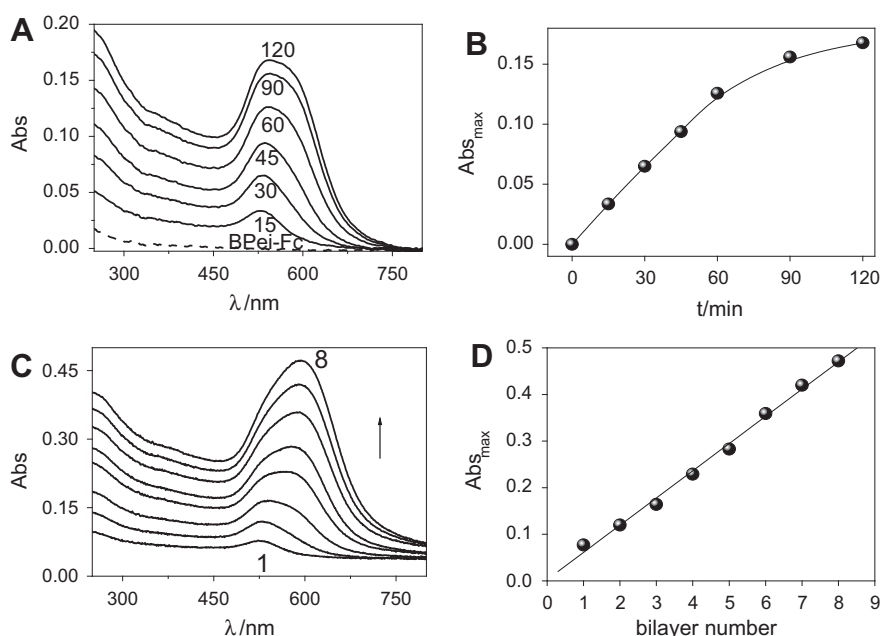

Fig. 4. (A) Spectral curves of Quartz/(HBPei-Fc/Au-NPs) for increasing adsorption time of Au-NPs from 15 to 120 min (▬). (B) Abs_{max} as a function of adsorption time. (C) Spectral curves of Quartz/(HBPei-Fc/Au-NPs)$_n$ as a function of bilayer number. (D) Abs_{max} as a function of bilayer number.
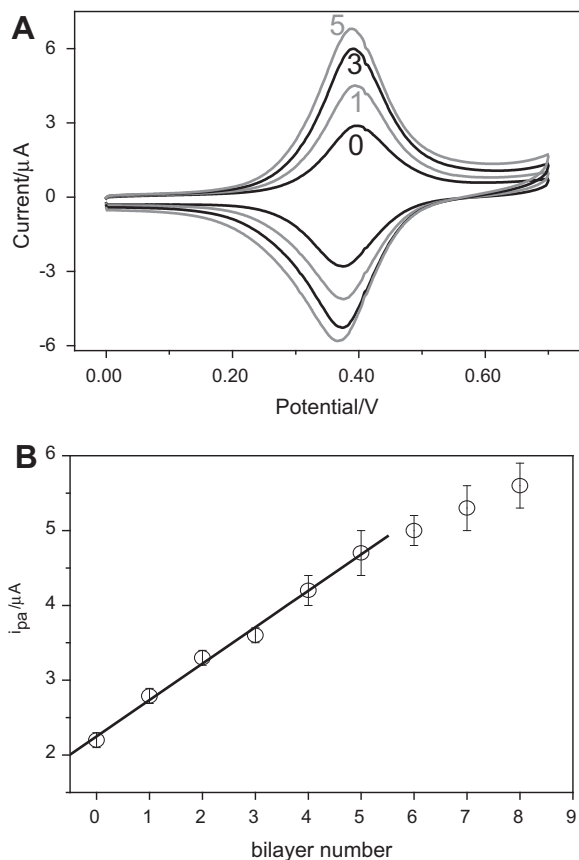
Fig. 5. (A) Cyclic voltammograms at $0.100\ V\ s^{-1}$ of Au/MPS/(HBPei-Fc/Au-NPs)$_n$/HBPei-Fc electrodes with increasing number of bilayers. (B) Variation in i_{pa} vs. number of bilayers. Supporting electrolyte: $0.200\ M\ NaClO_4$ at pH 6.00. The potential (V) is reported vs. (Ag/AgCl/3 mol dm^{-3} NaCl).
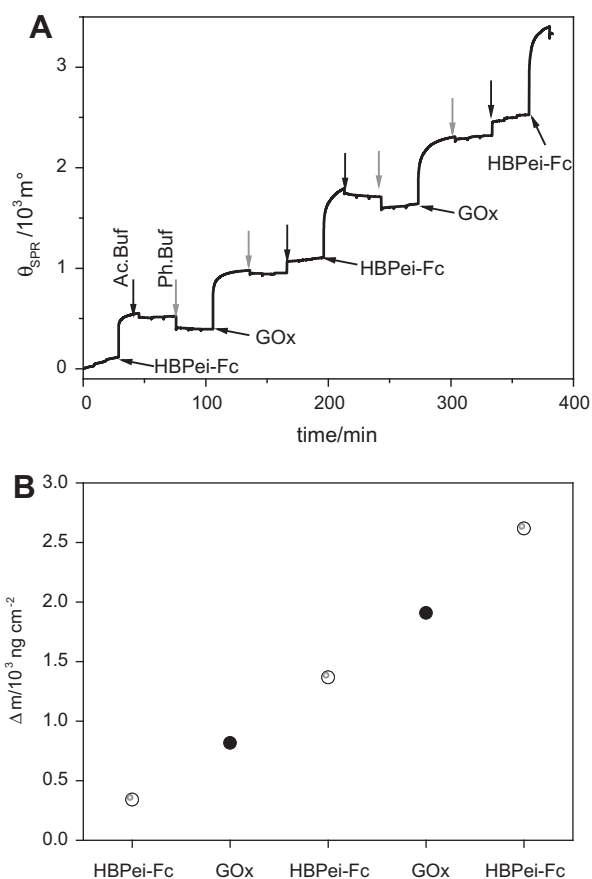

Fig. 6. (A) Sensorgrams obtained during the construction of the self-assembled multilayer of (HBPei-Fc/GOx)$_m$ at an Au/MPS surface. (B) Variation of adsorbed mass of HBPei-Fc (○) and GOx (●). Adsorption conditions: HBPei-Fc $3.0\ mg\ mL^{-1}$, GOx $1.0\ mg\ mL^{-1}$.

model for the construction of (HBPei-Fc/GOx)$_m$ multilayers at gold surfaces modified with MPS. We also evaluate the construction of multilayers with horseradish peroxidase, (not shown).

3.3.1. Evaluation of glucose oxidase adsorption

The construction of the multilayers was analyzed in situ by SPR. Fig. 6A shows the sensorgram obtained, where the arrows indicate when the electrolyte was added to the cell. The experiment starts recording a base line in 0.200 M acetate buffer (Phos. Buff.) solution at pH 5.00. After HBPei-Fc is injected, a change in the resonance angle is observed because of the polymer adsorption. To remove the weakly bound polymer, the surface is washed with 0.200 M acetate buffer solution at pH 5.00 until a stationary response is obtained. A change of electrolyte solution is performed to record the base line in 0.050 M phosphate buffer solution at pH 7.40. Then, GOx is injected, and a new increase in the resonance angle is observed as result of enzyme immobilization. To remove weakly bound GOx, the surface is washed with the phosphate buffer. The procedure is repeated to obtain the structure with the desired number of layers. The variation in the SPR angle, $\Delta\theta_{SPR}$, is measured as the difference in the signal recorded in buffer before and after the adsorption of each polyelectrolyte. The amount of polymer and enzyme immobilized on the surface was calculated by considering each $120\ m°$ of SPR angle displacement as $100\ ng\ cm^{-2}$ of adsorbed polyelectrolyte [26]. The values are presented in Fig. 6B. The surface coverage of GOx, (Γ_{GOx}), determined from the mass of protein adsorbed, was $(3.0 \pm 0.2) \times 10^{-12}$ mol cm^{-2} and $(3.4 \pm 0.2) \times 10^{-12}$ mol cm^{-2} for the first and second layers of GOx, respectively. These values are almost twice the

values that correspond to a closely packed monolayer of GOx, 1.7×10^{-12} mol cm^{-2} [44]. These results indicate that the protein is most likely aggregated on the polymeric layer.

To obtain kinetic information about the adsorption process of HBPei-Fc and GOx, we analyzed the time variation of the SPR mass according to a double exponential kinetic law, Eq. (2):

$$\Delta m = A_1 \left(1 - e^{-k_1 t}\right) + A_2 \left(1 - e^{-k_2 t}\right) \qquad (2)$$

where A_1 and A_2 correspond to the maximum Δm values for each adsorption step, and k_1 and k_2 stand for the time constants of two different kinetic steps in the adsorption process [2]. These double-exponential binding curves have been explained as representing nonspecific adsorption, conformational changes, the presence of two or more populations of binding site, or steric hindrance [2]. Fig. S7A shows the SPR mass transients for the first, second and third layers of HBPei-Fc, while Fig. S7B presents the profiles for the first and second layers of GOx obtained during the construction of the (HBPei-Fc/GOx)$_m$ multilayer. The best fits obtained with Eq. (2) are included in both figures in full lines. Very low residuals between the experimental and theoretical values were obtained, which suggested good fits that were independent of the initial values used for the fitting procedure. A single-exponential law, corresponding to a Langmuir type adsorption, was also tested and resulted in very poor fits. The values of the parameters obtained from the fits are included in Table 3. As the number of layer increases, A_1 and A_2 increase, in agreement with the tendency observed in Fig. 6B, while the adsorption rate constant k_1 decreases and k_2 remains almost constant.
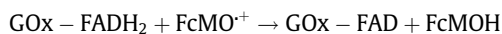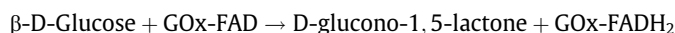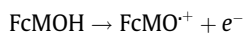
Table 3
Evolution of the adsorption constant values of (HBPei-Fc/GOx)$_m$ multilayer.[a]

m	A_1 ng cm^{-2}	$k_1/10^{-2}$ s^{-1}	A_2 ng cm^{-2}	$k_2/10^{-3}$ s^{-1}
0.5	285 ± 2	10.7 ± 0.3	82 ± 1	2.7 ± 0.2
1	355 ± 1	7.1 ± 0.1	130 ± 1	2.5 ± 0.5
1.5	347 ± 1	6.5 ± 0.1	249 ± 1	2.2 ± 0.4
2	373 ± 1	3.4 ± 0.4	246 ± 1	1.9 ± 0.2

[a] Multilayers were adsorbed at Au/MPS surface.

3.3.2. Catalytic activity of immobilized glucose oxidase

We evaluate the surface concentration of electroactive GOx, Γ^*_{GOx}, adsorbed at Au/MPS/HBPei-Fc using Bourdillon's method with FcMOH in solution as a redox regenerator in the absence of oxygen. Γ^*_{GOx} corresponds to the number of proteins adsorbed that can be electrochemically connected or electrochemically assessable [44]. The catalytic current, i_{cat}, was determined at Au/MPS/HBPei-Fc/GOx as the difference between the values obtained in the presence and absence of glucose. A well-defined S-shaped catalytic wave was obtained (Fig. S8A of Supporting information) because of GOx catalyzed oxidation of glucose, according to the following well-known mechanism [44]:

$$FcMOH \rightarrow FcMO^{\cdot+} + e^-$$

$$\beta\text{-D-Glucose} + GOx\text{-}FAD \rightarrow D\text{-glucono-}1,5\text{-lactone} + GOx\text{-}FADH_2$$

$$GOx - FADH_2 + FcMO^{\cdot+} \rightarrow GOx - FAD + FcMOH$$

Γ^*_{GOx} was calculated from this response using Eq. (3):

$$i_{cat} = \frac{nFAk_3\Gamma^*_{GOx}[FcMO^{\cdot+}]}{1 + k_3[FcMO^{\cdot+}]\left(\frac{1}{k_2} + \frac{1}{k_{red}[Glu]}\right)} \quad (3)$$

where [FcMO$^{\cdot+}$] and [Glu] are the concentrations of the oxidized mediator and substrate, respectively, and $k_{red} = k_1k_2/(k_{-1} + k_2)$. The constant values considered were $k_2 = 780$ s^{-1}, $k_3 = (6.2 \pm 0.5) \times 10^6$ M^{-1} s^{-1}, and $k_{red} = 1.2 \times 10^4$ M^{-1} s^{-1} [45]. We consider [FcMO$^{\cdot+}$] = [FcMOH]$_{bulk}$ because i_{cat} was measured at a high enough anodic potential (0.34 V vs. Ag/AgCl/3 mol dm^{-3} NaCl electrode). The stationary value of i_{cat} and Γ^*_{GOx} were 0.41 μA and $(2.1 \pm 0.1) \times 10^{-13}$ mol cm^{-2}, respectively. From the comparison between the amount of adsorbed enzyme determined by SPR, Γ_{GOx}, and the quantity of electrochemically active enzyme, Γ^*_{GOx}, we can conclude that only 7% of the immobilized enzyme is electrochemically assessable. Several reasons could explain this result: (1) aggregation of the protein, as was indicated previously, (2) electrostatic repulsion between [FcMO$^{\cdot+}$] and the positively charged HBPei-Fc around the enzyme, which most likely reduces the accessibility of the oxidized redox mediator to the active site of the enzyme [44] and (3) restricted diffusion of the redox mediator due to the way in which the layer system is ordered. In multilayer polyelectrolytes, where the polymers are not interpenetrated, the apparent diffusion coefficient, D_{app}, is much lower than in interdiffusive systems [45]. The linear increase in mass as a function of the adsorbed layer, as shown in Fig. 6B, suggests that (HBPei-Fc/GOx)$_m$ multilayers grow linearly, and consequently, the diffusion of FcMOH through the structure could be reduced.

HBPei-Fc was also tested as a possible regenerator of the enzyme in the presence of glucose in deoxygenated solutions. No catalytic responses were observed regardless of the medium used for GOx adsorption and measurements (Supporting information S8B). The lack of response cannot be attributed to inefficient adsorption of the protein at HBPei-Fc. We determined Γ_{GOx} experimentally and obtained the following values: 5.6×10^{-12} mol cm^{-2}, 3.0×10^{-12} mol cm^{-2} and 2.9×10^{-12} mol cm^{-2} in 0.200 M

solutions of sodium acetate, perchlorate and phosphate, respectively. The lack of enzyme regeneration could be the result of several factors: a decrease in the apparent diffusion coefficient of the redox groups, reduced segmental mobility of the polymer backbone after the adsorption of the protein due to the electrostatic interactions and/or a decrease in the accessibility to the redox center of GOx [19,45]. The difference in the regeneration capability of FcMOH in solution and HBPei-Fc is a consequence of the relatively higher mobility of diffusing FcMO$^{\cdot+}$ molecules in contrast to the rigidity of the HBPei-Fc polymer backbone. The formation of the encounter complex between the redox mediator and the enzyme active site is indeed expected to be much more rapid because of the smaller size of FcMO$^{\cdot+}$ than the polymer chain linked to ferrocenium cations.

4. Conclusions

We characterize the adsorption and electrochemical response of a ferrocenyl-modified polymer obtained from hyperbranched poly(ethylenimine) of a high molecular weight. The effect of the ionic strength, pH and nature of the anion of the supporting electrolyte was analyzed.

A high density of positive charges on the HBPei-Fc backbone makes it an excellent support for layer-by-layer construction of structures containing metallic nanoparticles. The results demonstrate a strong interpenetration between the layers that favors good electrical interconnection between the Fc groups of the polymer. The growth of the assemblies is uniform, and Au-NPs can efficiently tunnel electrons within the film. Additionally, the electrostatic adsorption of GOx on the modified polymer was evaluated. The surface coverage of the enzyme was almost twice the value corresponding to a closely packed monolayer of GOx. Electrochemical studies using a redox regenerator in solution confirm that the immobilized enzymes partially retain their catalytic activity, but under the configuration used for the construction of the HBPei-Fc multilayer, the polycation is not able to regenerate the enzyme. We are currently evaluating alternative constructions of multilayered structures based on the use of gold nanoparticles to improve the catalytic response.

Due to the simplicity, stability and versatility of the LbL self-assembled method, as well as the electrochemical response of the polymer and the amount of enzyme adsorbed, these results are very attractive for multi-functional applications.

Appendix A. Supplementary material

Supplementary data associated with this article can be found, in the online version, at http://dx.doi.org/10.1016/j.jelechem.2013.11.018.

References

[1] A. Akhoury, L. Bromberg, T.A. Hatton, Interplay of electron hopping and bounded diffusion during charge transport in redox polymer electrodes, J. Phys. Chem. B 117 (2013) 333–342.
[2] N.F. Ferreyra, L. Coche-Guérente, P. Labbé, E.J. Calvo, V.M. Solís, Electrochemical behavior of nitrate reductase immobilized in self-assembled structures with redox polyviologen, Langmuir 19 (2003) 3864–3874.

[3] C. Gaviglio, F. Battaglini, Hydrogen peroxide detection under physiological conditions by prussian blue stabilized using a polyelectrolyte-surfactant complex matrix, Sens. Actuators B 182 (2013) 53–57.

[4] T.V. Thanga, C. Cougnon, Redox properties and reactivity of a polythiophene-modified electrode in presence of ferrocene in solution or fixed onto the polymer network, J. Electroanal. Chem. 657 (1–2) (2011) 79–83.

[5] M.L. Cortez, G.A. González, F. Battaglini, An electroactive versatile matrix for the construction of sensors, Electroanalysis 23 (2011) 156–160.

[6] R. Gracia, D. Mecerreyes, Polymers with redox properties: materials for batteries, biosensors and more, Polym. Chem. 4 (2013) 2206–2214.

[7] J. Song, D. Janczewski, Y. Ma, L. van Ingen, C.E. Sim, Q. Goh, J. Xu, G.J. Vancso, Electrochemically controlled release of molecular guests from redox responsive polymeric multilayers and devices, Eur. Polym. J. 49 (2013) 2477–2484.

[8] B. C., Özer, H. Özyörük, S. S. Celebi, A. Yıldız. Amperometric enzyme electrode for free cholesterol determination prepared with cholesterol oxidase immobilized in poly(vinylferrocenium) film, Enzyme Microb. Technol. 40 (2007) 262–265.

[9] W. Yang, H. Zhou, C. Sun, Synthesis of ferrocene-branched chitosan derivatives: redox polysaccharides and their application to reagentless enzyme-based biosensors, Macromol. Rapid Comm. 28 (2007) 265–270.

[10] F. Zuo, C. Luo, X. Ding, Z. Zheng, X. Cheng, Y. Penga, Redox-responsive inclusion complexation between β-cyclodextrin and ferrocene-functionalized poly(N-isopropylacrylamide) and its effect on the solution properties of this polymer, Supramol. Chem. 20 (2008) 559–564.

[11] L. Deng, Y. Liu, G. Yang, L. Shang, D. Wen, F. Wang, Z. Xu, S. Dong, Molecular "wiring" glucose oxidase in supramolecular architecture, Biomacromolecules 8 (2007) 2063–2071.

[12] Y. Himuro, M. Takai, K. Ishihara, Poly(vinylferrocene-co-2-hydroxyethyl methacrylate) mediator as immobilized enzyme membrane for the fabrication of amperometric glucose sensor, Sens. Actuators B 139 (2009) 122–127.

[13] Z. Liu, M. Cardosi, J. Rodgers, G. Lillie, L. Simpson, Synthesis and study of copolymer of vinylferrocene, acrylamide and 2-(diethylamino)ethyl methacrylate as a polymeric mediator for electrochemical biosensors, React. Funct. Polym. 70 (2010) 715–725.

[14] B. Lal, A. Badshah, A.A. Altaf, N. Khan, S. Ullah, Miscellaneous applications of ferrocene-based peptides/amides, Appl. Organomet. Chem. 25 (2011) 843–855.

[15] M. Şenel, E. Çevik, M.F. Abasıyanık, A Novel amperometric hydrogen peroxide biosensor based on catalase immobilization on poly(glycidyl methacrylate-co-vinylferrocene), Anal. Bioanal. Chem. 3 (2011) 14–25.

[16] M.F. Abasıyanık, M. Şenel, Immobilization of glucose oxidase on reagentless ferrocene-containing polythiophene derivative and its glucose sensing application, J. Electroanal. Chem. 639 (2010) 21–26.

[17] M. Şenel, E. Çevika, M.F. Abasıyanık, Amperometric hydrogen peroxide biosensor based on covalent immobilization of horseradish peroxidase on ferrocene containing polymeric mediator, Sens. Actuators B 145 (2010) 444–450.

[18] S.A. Merchant, T.O. Tran, M.T. Meredith, T.C. Cline, D.T. Glatzhofer, D.W. Schmidtke, High-sensitivity amperometric biosensor based on ferrocene-modified linear poly(ethylenimine), Langmuir 13 (2009) 7736–7742.

[19] S.A. Merchant, M.T. Meredith, T.O. Tran, D.B. Brunski, M.B. Johnson, D.T. Glatzhofer, D.W. Schmidtke, Effect of mediator spacing on electrochemical and enzymatic response of ferrocene redox polymers, J. Phys. Chem. C 114 (2010) 11627–11634.

[20] M.T. Meredith, D.P. Hickey, J.P. Redeman, D.W. Schmidtke, D.T. Glatzhofer, Effects of ferrocene methylation on ferrocene-modified linear poly(ethylenimine) bioanodes, Electrochim. Acta 92 (2013) 226–235.

[21] J.L. DeLuca, D.P. Hickey, D.A. Bamper, D.T. Glatzhofer, M.B. Johnson, D.W. Schmidtke, Layer-by-layer assembly of ferrocene-modified linear polyethylenimine redox polymer films, Chem. Phys. Chem 14 (2013) 2149–2158.

[22] X. Liu, F. Wang, S. Han, L. Shi, G. Xua, Self-assembly of gold nanoparticles/electroactive polyelectrolyte multilayer films for tunable electrocatalysis, Electroanalysis 22 (2010) 963–968.

[23] G. De la Cruz, H. Schüle, J. Losada, M.P. García-Armada, H. Frey, B. Alonso, C.M. Casado, Electrocatalytic properties of carbosilane-based hyperbranched polymers functionalized with interacting ferrocenyl units, Eur. J. Inorg. Chem. (2013) 44–53.

[24] G. Khlebtsov, Determination of size and concentration of gold nanoparticles from extinction spectra, Anal. Chem. 80 (2008) 6620–6625.

[25] S.A. Merchant, D. Glatzhofer, D.W. Schmidtke, Effects of electrolyte and pH on the behavior of cross-linked films of ferrocene-modified poly(ethylenimine), Langmuir 23 (2007) 11295–11302.

[26] P. Ansorena, A. Zuzuarregui, A. Pérez-Lorenzo, M. Mujika, S. Arana, Comparative analysis of QCM and SPR techniques for the optimization of immobilization sequences, Sens. Actuators B 155 (2011) 667–672.

[27] M.M.O. Thotiyl, H. Basit, J.A. Sánchez, C. Goyer, L. Coche-Guerente, P. Dumy, S. Sampatha, P. Labbé, J-C. Moutet, Multilayer assemblies of polyelectrolyte-gold nanoparticles for the electrocatalytic oxidation and detection of arsenic (III), J. Colloid Interface Sci. 383 (2012) 130–139.

[28] A.W. Bott, Electrochemical techniques for the characterization of redox polymers, Curr. Sep. 19 (2001) 71–75.

[29] M. Tagliazucchi, E.J. Calvo, I. Szleifer, Redox and acid-base coupling in ultrathin polyelectrolyte films, Langmuir 24 (2008) 2869–2877.

[30] E. Laviron, L. Roullier, General expression of the linear potential sweep voltammogram for a surface redox reaction with interactions between the adsorbed molecules. Applications to modified electrodes, J. Electroanal. Chem. 115 (1980) 65–74.

[31] M. E.G. Lyons, G.P. Keeley, Carbon nanotube based modified electrode biosensors. Part 1.Electrochemical studies of the flavin group redox kinetics at SWCNT/glucose oxidase composite modified electrodes, Int. J. Electrochem. Sci. 3 (2008) 819–853.

[32] G.N.M. Ferreira, A.C. da-Silva, B. Tomé, Acoustic wave biosensors: physical models and biological applications of quartz crystal microbalance, Trends Biotechnol. 27 (2009) 689–697.

[33] D.J. Schmidt, F.C. Cebeci, Z.I. Kalcioglu, S.G. Wyman, C. Ortiz, K.J. van Vliet, P.T. Hammond, Electrochemically controlled swelling and mechanical properties of a polymer nanocomposite, ACS Nano 3 (2009) 2207–2216.

[34] M. Tagliazucchi, D. Grumelli, C. Bonazzola, E.J. Calvo, Oxidation-reduction dynamics in layer-by-layer self-assembled redox polyelectrolyte multilayer modified electrodes, J. Nanosci. Nanotechnol. 6 (2006) 1731–1740.

[35] R. Zahn, F. Boulmedais, J. Vörös, P. Schaaf, T. Zambelli, Ion and solvent exchange processes in PGA/PAH polyelectrolyte multilayers containing ferrocyanide, J. Phys. Chem. B 114 (2010) 3759–3768.

[36] C. Bunte, O. Prucker, T. Köing, J. Rühe, Enzyme containing redox polymer networks for biosensors or biofuel cells: a photochemical approach, Langmuir 26 (2010) 6019–6027.

[37] E.J. Calvo, A. Wolosiuk, Donnan permselectivity in layer-by-layer self-assembled redox polyelectrolye thin films, JACS 124 (2002) 8490–8497.

[38] R.A. Ghostine, M.Z. Markarian, J.B. Schlenoff, Asymmetric growth in polyelectrolyte multilayers, JACS 135 (2013) 7636–7646.

[39] Sh. Tokonami, Y. Yamamoto, H. Shiigi, T. Nagaoka, Synthesis and bioanalytical applications of specific-shaped metallic nanostructures: A review, Anal. Chim. Acta 716 (2012) 76–91.

[40] F. Terzi, C. Zanardi, B. Zanfrognini, L. Pigani, R. Seeber, J. Lukkari, T. Ääritalo, J. Kankare, Preparation and characterization of redox multilayer film containing Au nanoparticles, J. Phys. Chem. 113 (2009) 4868–4874.

[41] W. Yuan, C.M. Li, Direct modulation of localized surface plasmon coupling of Au nanoparticles on solid substrates via weak polyelectrolyte-mediated layer-by-layer self assembly, Langmuir 25 (2009) 7578–7585.

[42] M.V. Bracamonte, S. Bollo, P. Labbé, G.A. Rivas, N.F. Ferreyra, Quaternized chitosan as support for the assembly of gold nanoparticles and glucose oxidase: Physicochemical characterization of the platform and evaluation of its biocatalytic activity, Electrochim. Acta 56 (2011) 1316–1322.

[43] C.E. Dowdy, M.C. Leopold, Enhanced electrochemistry of nanoparticle-embedded polyelectrolyte films: Interfacial electronic coupling and distance dependence, Thin Solid Films 519 (2010) 790–796.

[44] N.F. Ferreyra, L. Coche-Guérente, P. Labbé, Construction of layer-by-layer self-assemblies of glucose oxidase and cationic polyelectrolyte onto glassy carbon electrodes and electrochemical study of the redox-mediated enzymatic activity, Electrochim. Acta 49 (2004) 477–484.

[45] R. Zahn, G. Coullerez, J. Vörös, T. Zambelli, Effect of polyelectrolyte interdiffusion on electron transport in redox-active polyelectrolyte multilayers, J. Mater. Chem. 22 (2012) 11073–11078.